Nuclear Engineering and Technology 52 (2020) 2630–2637

Contents lists available at ScienceDirect

Nuclear Engineering and Technology

journal homepage: www.elsevier.com/locate/net

Original Article

Dynamic analysis of multi-functional maintenance platform based on Newton-Euler method and improved virtual work principle

Dongyi Li [a, b, c], Kun Lu [a], Yong Cheng [a, c], Wenlong Zhao [a, c], Songzhu Yang [a, c], Yu Zhang [a, c], Junwei Li [a, b], Shanshuang Shi [a, c, *]

[a] Institute of Plasma Physics, Chinese Academy of Sciences, Hefei, China
[b] University of Science and Technology of China, Hefei, China
[c] Anhui Extreme Environment Robot Engineering Laboratory, Hefei, China

ARTICLE INFO

Article history:
Received 21 January 2020
Received in revised form
27 March 2020
Accepted 14 April 2020
Available online 5 June 2020

Keywords:
China Fusion engineering test reactor
Divertor
Multi-functional maintenance platform
3-RPS parallel Robot
Dynamic analysis
ADAMS simulation

ABSTRACT

The structure design of divertor Multi-Functional Maintenance Platform (MFMP) actuated by hydraulic system for China Fusion Engineering Test Reactor (CFETR) was introduced in this paper. The model of MFMP was established according to maintenance requirements. In this paper, Newton-Euler method and the improved virtual work principle were used, the equivalent driving force of each actuator was obtained through the equivalent Jacobian inverse matrix derived from velocity relationship among the components. The accuracy of the model was verified by ADAMS simulation. The stability control of the heavy-duty components driven by hydraulic cylinders based on Newton-Euler method and improved virtual work principle was established.

1. Introduction

The MFMP is a remote handling maintenance device for the divertors of CFETR, which mainly includes functions of cooling pipeline cutting and welding, divertor fixing and unlocking, and divertor replacing etc. [1–8]. In the process of carrying the divertor, the toroidal moving driver (TMD) at the bottom of the MFMP contacts with the circular track fixed on the vacuum vessel can take the divertor moving in toroidal direction. And the MFMP can lift the divertor through the moving platform driven by hydraulic cylinders [9].

The dynamic analysis of 3-RPS parallel robot of MFMP is studied in this paper. For parallel robots, the dynamic analysis has been studied widely [10–12]. Calculating the forces and torques required for each actuator of the parallel robot in different position is the fundamental task for dynamic, static analysis and control of the parallel robot, including forward dynamics and inverse dynamics. At present, relatively perfect methods for establishing dynamic models include Newton-Euler method, Lagrange method [13,14], Kane method, virtual work principle etc. Newton-Euler method is used to study a single component. Newton's law and Euler equation are used to set the mechanism balance equation. Although this method needs to calculate a large number of equations, it can be used to calculate the internal forces between components, which is very useful for the study of a single parallel mechanical limb. The Lagrange method only requires the kinetic energy and potential energy of the system, and it does not need to calculate the internal force. However, the selection of generalized coordinates is very important. For parallel robots, joint constraints make the selection of generalized coordinates difficult. The Kane method is especially applicable to the solution of the forward dynamic solution by projecting the component forces. In the virtual work principle, it is assumed that the parallel robot is statically balanced, the actual displacement is replaced by the virtual displacement$\delta\boldsymbol{\chi}$. The relationship between the driving force and the external force can be deduced by the conclusion that the sum of virtual work done by the driving force and the external force is zero [12,15]. $\delta\boldsymbol{\chi} = [\delta x, \delta y, \delta z, \delta\theta_x, \delta\theta_y, \delta\theta_z]^T$ represents the virtual displacement of the moving platform. $\delta\boldsymbol{q} = [\delta_{q1}, \delta_{q2}, \delta_{q3}, \ldots, \delta_{qm}]^T$represents the virtual displacement of the driving joint of the parallel manipulator

* Corresponding author. Institute of Plasma Physics, Chinese Academy of Sciences, Hefei, China.
E-mail address: shiss@ipp.ac.cn (S. Shi).

https://doi.org/10.1016/j.net.2020.04.017

with m actuators. $\boldsymbol{\tau} = [\tau_1, \tau_2, \tau_3, \ldots, \tau_m]^T$ represents the driving force of driving joints. $\boldsymbol{F} = [\boldsymbol{fn}]^T$ is external force and external torque matrices ($\boldsymbol{f} = [f_x f_y f_z]^T$ is external force, $\boldsymbol{n} = [n_x n_y n_z]^T$ is external torque matrix.). The sum of virtual work done by driving force and external force is: $\delta w = \boldsymbol{\tau}^T \delta \boldsymbol{q} - \boldsymbol{F}^T \delta \boldsymbol{\chi} = 0$. In parallel robots, $\dot{\boldsymbol{q}} = \boldsymbol{J}\dot{\boldsymbol{\chi}}$, and $\boldsymbol{J}$ is Jacobian matrix. Combining with $\dot{\boldsymbol{q}} = \boldsymbol{J}\dot{\boldsymbol{\chi}}$, equation $\delta \boldsymbol{q} = \boldsymbol{J}\delta\boldsymbol{\chi}$ is gained. Substituting $\delta \boldsymbol{q} = \boldsymbol{J}\delta\boldsymbol{\chi}$ into $\delta w = \boldsymbol{\tau}^T \delta \boldsymbol{q} - \boldsymbol{F}^T \delta \boldsymbol{\chi} = 0$, $\delta w = (\boldsymbol{\tau}^T \boldsymbol{J} - \boldsymbol{F}^T)\delta\boldsymbol{\chi} = 0$ is gained. Then, the following equation that solves driving force can be derived: $\boldsymbol{\tau} = \boldsymbol{J}^{-T}\boldsymbol{F}$.

However, the key problem with this traditional virtual work principle is that driving force $\boldsymbol{\tau}$ cannot be solved because Jacobi matrix $\boldsymbol{J}$ is not full rank matrix in 3-RPS parallel robot [16]. In this paper, a method is put forward that the equivalent inverse Jacobian matrix $\mathbf{K}$ can be calculated via the velocity relationships between moving platform and actuators, cylinder mass center and actuator, piston rod mass center and actuator. And the equivalent driving force actuating moving platform, the cylinder and the piston rod is solved by improved principle of virtual work method $\boldsymbol{\tau} = \mathbf{K}^T\boldsymbol{F}$, in the meanwhile, the driving force of actuators is gained.

2. The model of CFETR divertor MFMP

The CFETR divertor MFMP is mainly divided into three parts: internal and external TMD, the moving platform of 3-RPS parallel robot and the main body of maintenance platform, as shown in Fig.1. The circular moving hydraulic cylinders in the internal and external TMD cooperate with each other to move the MFMP along the track to realize the toroidal movement of the divertor. The top support system of internal and external TMD can achieve lifting, rotating and other movements of moving platform of 3-RPS parallel robot. There is a small hydraulic power station inside the main body of maintenance platform providing sufficient hydraulic power. The linear motor provides thrust locking and unlocking the inner and outer track.

The internal and external TMD consists of three parts, as shown in Fig. 2(a) and (b) top support system (jacking cylinder), driving system and flexible roller. There are four hydraulic cylinders in the top support system of each TMD, and a total of eight hydraulic cylinders in the internal and external TMD work together to support the moving platform and carry the divertor. At bottom each cylinder is connected with the TMD by a revolute joint, and at upper end of each piston rod is connected with the bottom of the moving platform by a spherical joint. The driving system includes circular driving hydraulic cylinders and clamping cylinders.

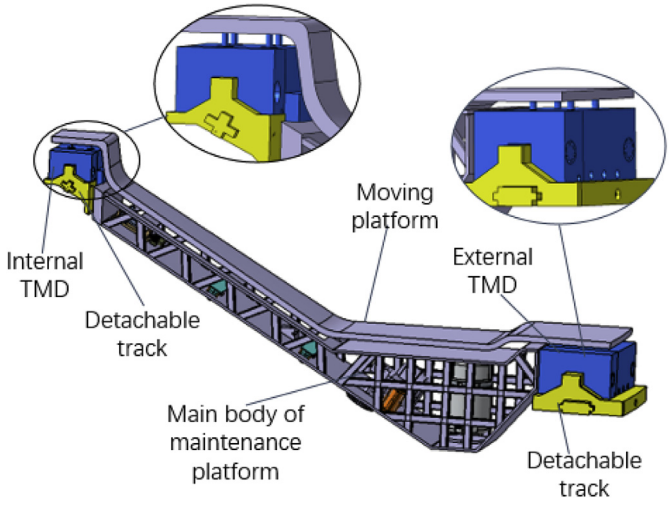

Fig. 1. The CFETR divertor MFMP.

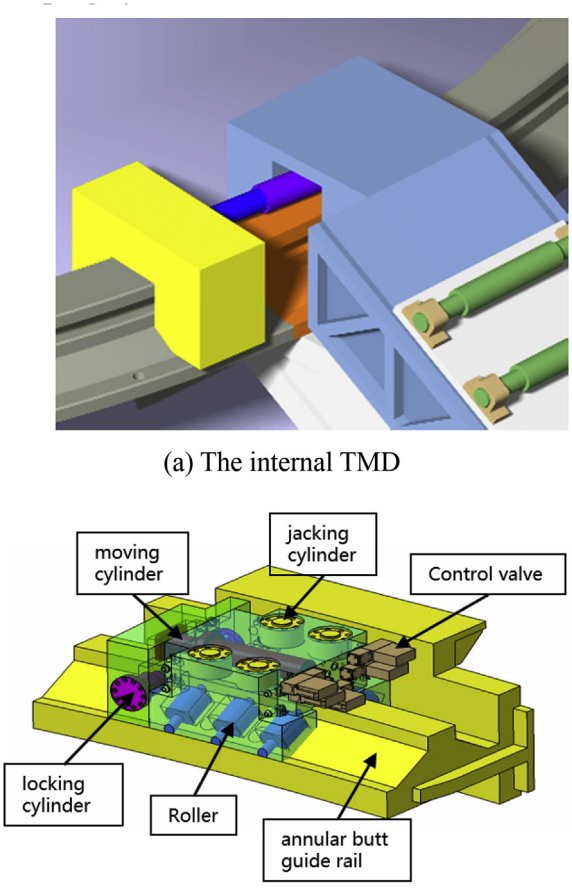

(a) The internal TMD

(b) The TMD model

Fig. 2. Toroidal moving driver (TMD). (a)The internal TMD. (b)The TMD model.

When mobile platform starts to move in toroidal direction, the driving rod of the circular moving hydraulic cylinder extends. After reaching the predetermined position, the clamp device of the TMD is clamped on the track by the locking cylinder. And circular driving hydraulic cylinder retracts to drive the MFMP and the divertor to move forward. When cylinder return to its minim position the clamping will release. With the repetition MFMP can intermittently move along the track. When the MFMP arrives at the lower maintenance port, the top support system supports the moving platform and adjusts the divertor's angle and position accordingly. The flexible roller is composed of rollers and disk springs. The disc springs enable the rollers to automatically adjust the angle, making better contact on the face of the track and reducing friction during the toroidal movement.

The removable track is an important part of the track in the vacuum vessel as shown in Fig. 3(a) and (b) [17]. When the removable track enters the vacant position in the toroidal track of the vacuum vessel, the linear motor in the main body of maintenance platform pushes the fixed device inside the fixed track. Then the removable track and the fixed track lock each other, the MFMP can move along the toroidal track in vacuum vessel.

3. Simplified model of MFMP

According to the actual functional requirements, without considering the deformation of the moving platform, the MFMP can be simplified as a 3-RPS parallel robot driven by three hydraulic

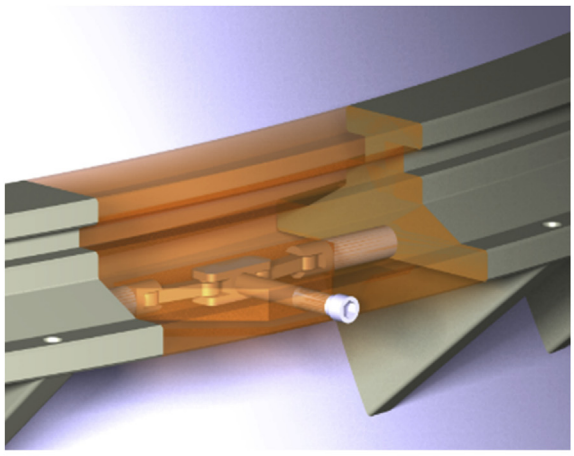

(a) Internal fixture in removable track

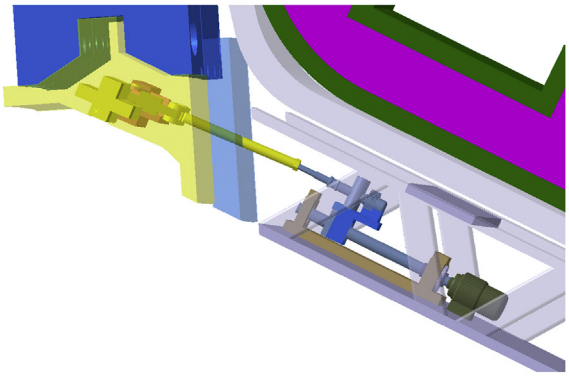

(b) The linear motor in MFMP

Fig. 3. Removable track. (a)Internal fixture in removable track. (b)The linear motor in MFMP

cylinders in 2 TMDs [18–20], as shown in Fig. 4. The internal TMD provides one driving force, and external TMD provides two driving forces.

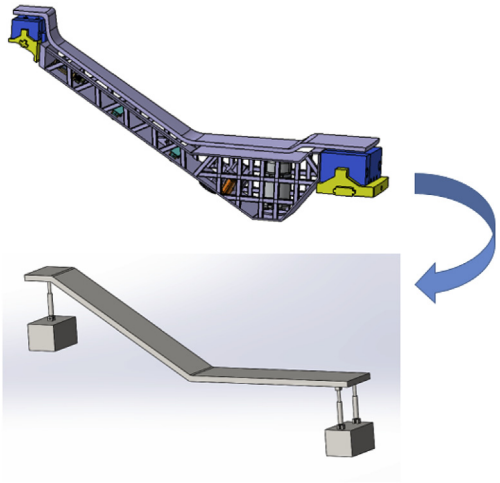

Fig. 4. RPS parallel robot.

4. Dynamic analysis of 3-RPS parallel robot

4.1. The solution for equivalent inverse jacobian matrix

In this section, the Newton-Euler method is used to derive the velocity conversion matrix between the actuators and the moving platform, the transformation matrix between the linear velocity of actuators and the actual velocity of the moving platform. Based on the above matrix, the equivalent inverse Jacobian matrix between the actuators and the moving platform is obtained. The velocity conversion matrix between cylinder/piston rod and moving platform can be derived, the equivalent inverse Jacobi matrix between cylinder/piston rod and moving platform can be obtained based on the above matrix.

As shown in Fig. 5 and Fig. 6 the reference coordinate system {A} A - XYZ is set in the center of the fixed platform. And the moving coordinate system {B} B - xyz is set in the center of the moving platform. $\hat{\boldsymbol{s}}_i$ is unit vector from point a_i in fixed platform to point b_i in moving platform. $\boldsymbol{r}_{ai}$ is unit vector from center point A of fixed platform to point a_i. $\boldsymbol{r}_{bi}$ is unit vector from center point A of moving platform to point b_i.

The linear velocity at the center point B of the moving platform is ${}^{A}\boldsymbol{V}_B$, the angular velocity is ${}^{A}\boldsymbol{\omega}_B$. The velocity at the spherical joint center b_i in the moving platform is ${}^{A}\boldsymbol{V}_{bi}$, and $\dot{\boldsymbol{L}}_i$ represents the velocity of the rod. v_M represents the velocity of MFMP toroidal movement.

Since the selected reference coordinate system will affect the representation of the vector, in order to distinguish the reference coordinate system of each parameter, the annotation on the upper left corner of the vector in this paper represents the corresponding coordinate system. If there is no annotation, the default reference coordinate system is the fixed coordinate system {A}.

4.1.1. The velocity transformation matrix between the actuators and the moving platform

For each spherical joint b_i of the moving platform, its velocity can be written as:

$$ {}^{A}\boldsymbol{V}_{bi} = \hat{\boldsymbol{s}}_i \dot{l}_i + \left({}^{A}\boldsymbol{\omega}_i \times \hat{\boldsymbol{s}}_i\right) l_i \qquad (4-1) $$

It can also be written as

$$ {}^{A}V_{bi} = {}^{A}\omega_B \times {}^{A}r_{bi} + {}^{A}V_B \qquad (4-2) $$

Where.

$\dot{l}_i$——linear velocity of each actuators,$i = 1, 2, 3$;

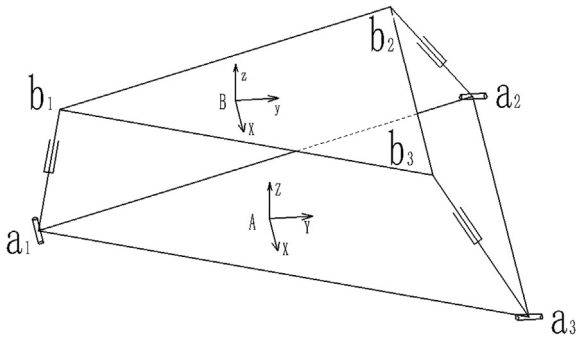

Fig. 5. Schematic diagram of 3-RPS parallel robot.

${}^{A}\boldsymbol{\omega}_i$——angular velocity of each actuators, $i = 1, 2, 3$.

Due to the RPS rod can't turn around its own axis, ${}^{A}\boldsymbol{\omega}_i \perp \hat{\boldsymbol{s}}_i$, ${}^{A}\boldsymbol{\varepsilon}_i \perp \hat{\boldsymbol{s}}_i$, equations (4-1) dotting $\hat{\boldsymbol{s}}_i$ can be simplified to:

$$\hat{s}_i n^{A} V_{bi} = \dot{l}_i \tag{4-3}$$

From equations (4-2) and (4-3), the following equation can be derived:

$$\dot{l}_i = \hat{\boldsymbol{s}}_i \cdot \left({}^{A}\boldsymbol{\omega}_i \times {}^{A}\boldsymbol{r}_{bi}\right) + \hat{\boldsymbol{s}}_i \cdot {}^{A}\boldsymbol{V}_B = \left[\hat{\boldsymbol{s}}_i^T \left({}^{A}\boldsymbol{r}_{bi} \times \hat{\boldsymbol{s}}_i\right)^T\right] \cdot \left[{}^{A}\boldsymbol{V}_B \, {}^{A}\boldsymbol{\omega}_B\right]^T \tag{4-4}$$

For the overall parallel robot, the following equation can be obtained:

$$\dot{\boldsymbol{L}} = \boldsymbol{J}_{1A} \cdot \begin{bmatrix} {}^{A}\boldsymbol{V}_B \\ {}^{A}\boldsymbol{\omega}_B \end{bmatrix} \tag{4-5}$$

Where, $\dot{\boldsymbol{L}} = [\dot{\boldsymbol{L}}_1 \dot{\boldsymbol{L}}_2 \dot{\boldsymbol{L}}_3]^T$.

$\boldsymbol{J}_{1A}$ is velocity transformation matrix between the actuators and the moving platform:

$$\boldsymbol{J}_{1A} = \begin{bmatrix} \hat{\boldsymbol{s}}_1^{\,T} & \left({}^{A}\boldsymbol{r}_{b1} \times \hat{\boldsymbol{s}}_1\right)^T \\ \hat{\boldsymbol{s}}_2^{\,T} & \left({}^{A}\boldsymbol{r}_{b2} \times \hat{\boldsymbol{s}}_2\right)^T \\ \hat{\boldsymbol{s}}_3^{\,T} & \left({}^{A}\boldsymbol{r}_{b3} \times \hat{\boldsymbol{s}}_3\right)^T \end{bmatrix}$$

For cross multiplication of both sides of equations (4-1) with $\hat{\boldsymbol{s}}_i$, the following equation can be derived:

$${}^{A}\boldsymbol{\omega}_i = \frac{\hat{\boldsymbol{s}}_i \times {}^{A}\boldsymbol{V}_{bi}}{l_i} \tag{4-6}$$

From equations (4-2) and (4-6), the following equation can be derived:

$${}^{A}\boldsymbol{\omega}_i = \frac{\hat{\boldsymbol{s}}_i}{l_i} \times \left({}^{A}\boldsymbol{\omega}_B \times {}^{A}\boldsymbol{r}_{bi} + {}^{A}\boldsymbol{V}_B\right) = \frac{1}{l_i}\left[\hat{\boldsymbol{s}}_{i\times} - \hat{\boldsymbol{s}}_{i\times} {}^{A}\boldsymbol{r}_{bi\times}\right] \cdot \left[{}^{A}\boldsymbol{V}_B \, {}^{A}\boldsymbol{\omega}_B\right]^T \tag{4-7}$$

Where, $\hat{\boldsymbol{s}}_{i\times}$ and ${}^{A}\boldsymbol{r}_{bi\times}$ denote skew-symmetric matrices derived from elements of vectors.

4.1.2. The transformation matrix between the linear velocity of the actuators and the actual velocity of the moving platform

Firstly, due to the limitation of the revolute joints, point b_1 on the moving platform cannot move along the X-axis and point b_2 cannot move along the Y-axis. Based on these two conditions, the relationship between the velocity of the moving platform ${}^{A}\boldsymbol{\omega}_B = [\omega_x \omega_y \omega_z]^T$ and the Euler angle $\theta = [\alpha, \beta, \gamma]^T$ of the moving platform can be deduced (In this paper, the Z-Y-X Euler angle is used).

The posture transformation matrix

$${}^{A}\boldsymbol{R}_B = \begin{bmatrix} c\alpha \cdot c\beta & c\alpha \cdot s\beta \cdot s\gamma - c\gamma \cdot s\alpha & s\alpha \cdot s\gamma + c\alpha \cdot c\gamma \cdot s\beta \\ c\beta \cdot s\alpha c\alpha \cdot c\gamma + s\alpha \cdot s\beta \cdot s\gamma c\gamma \cdot s\alpha \cdot s\beta - c\alpha \cdot s\gamma - s\beta & & \\ & c\beta \cdot s\gamma & c\beta \cdot c\gamma \end{bmatrix}$$

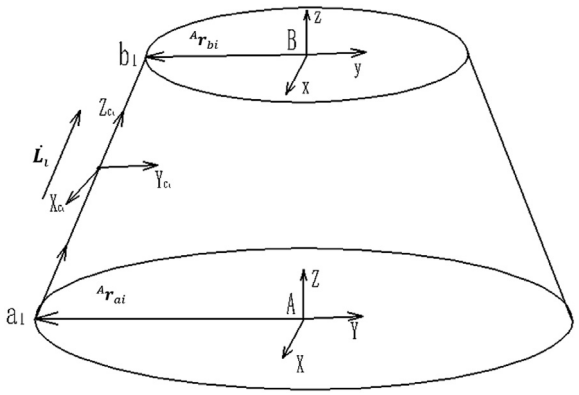

Fig. 6. Diagram of parameters of parallel robot.

Where, $c\theta = \cos\theta$, $s\theta = \sin\theta$.

The coordinates of points b_1 and b_2 were obtained, and the velocity of moving platform in X and Y axis was deduced:

$${}^{A}\boldsymbol{b}_1 = \begin{bmatrix} {}^{A}X_1 \\ {}^{A}Y_1 \\ {}^{A}Z_1 \end{bmatrix} = {}^{A}\boldsymbol{R}_B \, {}^{B}\boldsymbol{b}_1 + {}^{A}\boldsymbol{P} = {}^{A}\boldsymbol{R}_B \begin{bmatrix} {}^{B}X_1 \\ {}^{B}Y_1 \\ {}^{B}Z_1 \end{bmatrix} + \begin{bmatrix} {}^{A}X_O \\ {}^{A}Y_O \\ {}^{A}Z_O \end{bmatrix} = {}^{A}\boldsymbol{R}_B \begin{bmatrix} 0 \\ {}^{B}Y_1 \\ 0 \end{bmatrix} + \begin{bmatrix} {}^{A}X_O \\ {}^{A}Y_O \\ {}^{A}Z_O \end{bmatrix} \tag{4-8}$$

From equations (4-8), the following equation can be derived:

$${}^{A}X_1 = \sin\beta \sin\gamma \, {}^{B}Y_1 + {}^{A}X_O = 0 \tag{4-9}$$

It can be explicitly expressed by

$${}^{A}X_O = -\sin\beta \sin\gamma \, {}^{B}Y_1 \tag{4-10}$$

Calculating derivative of equations 4–10 with respect to time, the following equation can be derived:

$${}^{A}\boldsymbol{V}_{Bx} = -{}^{B}Y_1 \cos\beta \sin\gamma\dot{\beta} - {}^{B}Y_1 \sin\beta \cos\gamma\dot{\gamma} \tag{4-11}$$

in a similar way:

$$^{A}\boldsymbol{b}_2=\begin{bmatrix}^{A}X_2\\ ^{A}Y_2\\ ^{A}Z_2\end{bmatrix}=^{A}\boldsymbol{R}_B\,^{B}\boldsymbol{b}_2+^{A}\boldsymbol{P}=^{A}\boldsymbol{R}_B\begin{bmatrix}^{B}X_2\\ ^{B}Y_2\\ ^{B}Z_2\end{bmatrix}+\begin{bmatrix}^{A}X_O\\ ^{A}Y_O\\ ^{A}Z_O\end{bmatrix}=^{A}\boldsymbol{R}_B\begin{bmatrix}^{B}X_2\\ ^{B}Y_2\\ 0\end{bmatrix}+\begin{bmatrix}^{A}X_O\\ ^{A}Y_O\\ ^{A}Z_O\end{bmatrix} \quad (4-12)$$

$$^{A}Y_2=\cos\gamma\,^{B}Y_2+^{A}Y_O=0 \quad (4-13)$$

$$^{A}Y_O=-\cos\gamma\,^{B}Y_2 \quad (4-14)$$

Calculating derivative of equations 4–14 with respect to time, the following equation can be derived:

$$^{A}\boldsymbol{V}_{By}=^{B}Y_2\sin\gamma\dot{\gamma} \quad (4-15)$$

From the posture transformation matrix, the following equation can be derived:

$$^{A}\boldsymbol{\omega}_B=R(Z,\alpha)\begin{bmatrix}0\\0\\1\end{bmatrix}\dot{\alpha}+R(Z,\alpha)R(Y,\beta)\begin{bmatrix}0\\1\\0\end{bmatrix}\dot{\beta}+R(Z,\alpha)R(Y,\beta)R(X,\gamma)\begin{bmatrix}1\\0\\0\end{bmatrix}\dot{\gamma}=\begin{bmatrix}0&-\sin\alpha&\cos\alpha\cos\beta\\0&\cos\alpha&\sin\alpha\cos\beta\\1&0&-\sin\beta\end{bmatrix}\begin{bmatrix}\dot{\alpha}\\\dot{\beta}\\\dot{\gamma}\end{bmatrix} \quad (4-16)$$

In combination with equations (4), (4), (5), (5), (6), (6), (7), (7), (8), (8), (9), (9), (10), (10), (11), (11)–(15) and (4-16), the conversion relationship between six-dimensional velocity and three-dimensional velocity is obtained:

$$\begin{bmatrix}^{A}\boldsymbol{V}_B\\ ^{A}\boldsymbol{\omega}_B\end{bmatrix}=\boldsymbol{J}_{2A}\begin{bmatrix}^{A}\boldsymbol{V}_{Bz}\\ \dot{\beta}\\ \dot{\gamma}\end{bmatrix} \quad (4-17)$$

Where,

$$\boldsymbol{J}_{2A}=\begin{bmatrix}0&-^{B}Y_1\cos\beta\sin\gamma&0\\0&0&-^{B}Y_1\sin\beta\cos\gamma\\1&0&^{B}Y_2\sin\gamma\\0&0&0\\0&1&\cos\beta\\0&0&0\\0&0&-\sin\beta\end{bmatrix}$$

From equations (4-5) and (4-17), the following equation can be derived:

$$\dot{\boldsymbol{L}}=\boldsymbol{J}_A\begin{bmatrix}^{A}\boldsymbol{V}_{Bz}\\ \dot{\beta}\\ \dot{\gamma}\end{bmatrix} \quad (4-18)$$

It can also be expressed as

$$\boldsymbol{J}_A^{-1}\dot{\boldsymbol{L}}=\begin{bmatrix}^{A}\boldsymbol{V}_{Bz}\\ \dot{\beta}\\ \dot{\gamma}\end{bmatrix} \quad (4-19)$$

Where, $\boldsymbol{J}_A$ is the 3 × 3 dimensional velocity conversion matrix between the linear velocity of actuators and the actual velocity of the moving platform, $\boldsymbol{J}_A=\boldsymbol{J}_{1A}\boldsymbol{J}_{2A}$.

4.1.3. Velocity conversion matrix between cylinder/piston rod and moving platform

As shown in Fig. 7, the hydraulic actuators can be decomposed into two independent parts, and their masses are represented by m_{ci}(c for cylinder) and m_{pi}(p for piston) respectively. The position vectors of the two mass centers can be determined by the following equation:

$$\boldsymbol{p}_{ci}=^{A}\boldsymbol{r}_{ai}+h_{ci}\hat{\boldsymbol{s}}_i \quad (4-20)$$

$$\boldsymbol{p}_{pi}=^{A}\boldsymbol{r}_{ai}+(l_i-h_{pi})\hat{\boldsymbol{s}}_i \quad (4-21)$$

Where:

h_{ci}——Length from mass center of cylinder to revolve joint,
h_{pi}——Length from piston rod mass center to spherical joint.

Calculating derivative of equations 4–20 and (4-21) with respect to time, and get linear velocity expressions of cylinder and piston rod mass center:

$$\boldsymbol{V}_{ci}=h_{ci}(\boldsymbol{\omega}_i\times\hat{\boldsymbol{s}}_i) \quad (4-22)$$

$$\boldsymbol{V}_{pi}=(l_i-h_{pi})(\boldsymbol{\omega}_i\times\hat{\boldsymbol{s}}_i)+\dot{l}_i\hat{\boldsymbol{s}}_i \quad (4-23)$$

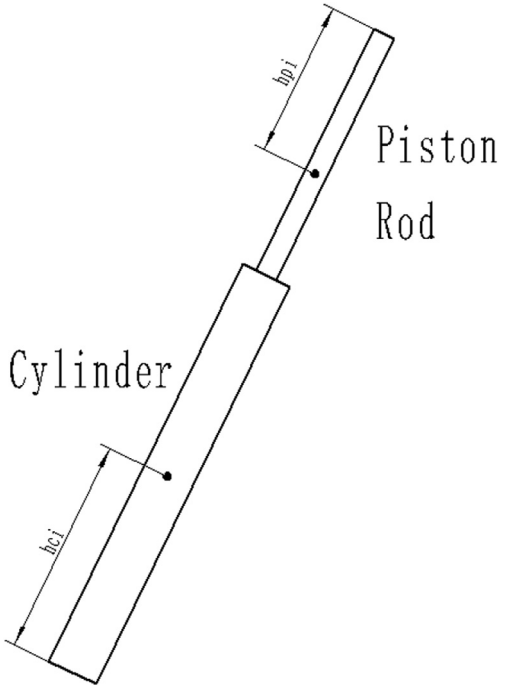

Fig. 7. The diagram of actuator parameters.

From equations (4-7) and (4-22) the relation between the velocity of cylinder and the velocity of moving platform can be derived:

$$\begin{bmatrix} \boldsymbol{V}_{ci} \\ \boldsymbol{\omega}_i \end{bmatrix} = \boldsymbol{J}_{ci} \begin{bmatrix} \boldsymbol{V}_B \\ \boldsymbol{\omega}_B \end{bmatrix} \quad (4-24)$$

Where, $\boldsymbol{J}_{ci}$ is conversion matrix between velocity of mass center of cylinder and velocity of moving platform:

$$\boldsymbol{J}_{ci} = \frac{1}{l_i}\left[-h_{ci}\widehat{\boldsymbol{s}}_{i\times}^2 \; h_{ci}\widehat{\boldsymbol{s}}_{i\times}^2 \boldsymbol{r}_{bi\times} \; \widehat{\boldsymbol{s}}_{i\times} - \widehat{\boldsymbol{s}}_{i\times}\boldsymbol{r}_{bi\times}\right]$$

In the same way, from equations 4-1,4-2,4-7 and (4-23), the relationship between the velocity of the piston rod and the velocity of the moving platform can be expressed as follows:

$$\begin{bmatrix} \boldsymbol{V}_{pi} \\ \boldsymbol{\omega}_i \end{bmatrix} = \boldsymbol{J}_{pi} \begin{bmatrix} \boldsymbol{V}_B \\ \boldsymbol{\omega}_B \end{bmatrix} \quad (4-25)$$

Where, $\boldsymbol{J}_{pi}$ is the transformation matrix between velocity of piston rod mass center and velocity of moving platform.

$$\boldsymbol{J}_{pi} = \begin{bmatrix} \boldsymbol{I} + \dfrac{h_{pi}\widehat{\boldsymbol{s}}_{i\times}^2}{l_i} & -\left(\boldsymbol{r}_{bi\times} + \dfrac{h_{pi}\widehat{\boldsymbol{s}}_{i\times}^2 \boldsymbol{r}_{bi\times}}{l_i}\right) \\ \dfrac{\widehat{\boldsymbol{s}}_{i\times}}{l_i} & -\dfrac{\widehat{\boldsymbol{s}}_{i\times}\boldsymbol{r}_{bi\times}}{l_i} \end{bmatrix}$$

4.1.4. Equivalent inverse jacobian matrix

From equations 4–17 and (4-19), the following equation can be derived:

$$\begin{bmatrix} {}^A\boldsymbol{V}_B \\ {}^A\boldsymbol{\omega}_B \end{bmatrix} = \bar{\boldsymbol{J}} \cdot \dot{\boldsymbol{L}} \quad (4-26)$$

Where, $\bar{\boldsymbol{J}} = \boldsymbol{J}_{2A} \cdot \boldsymbol{J}_A^{-1}$ represents the equivalent inverse Jacobian matrix between the velocity of the moving platform and the linear velocity of the actuators.

From equations 4–24 and (4-26), the following equation can be derived:

$$\begin{bmatrix} \boldsymbol{V}_{ci} \\ \boldsymbol{\omega}_i \end{bmatrix} = \bar{\boldsymbol{J}}_{ci} \cdot \dot{\boldsymbol{L}} \quad (4-27)$$

Where, $\bar{\boldsymbol{J}}_{ci} = \boldsymbol{J}_{ci} \cdot \bar{\boldsymbol{J}}$ represents the equivalent Jacobian inverse matrix between the velocity of the mass center of the cylinder and the linear velocity of the actuators.

Substituting equations 4–25 into equations 4–26, the following equation can be derived:

$$\begin{bmatrix} \boldsymbol{V}_{pi} \\ \boldsymbol{\omega}_i \end{bmatrix} = \bar{\boldsymbol{J}}_{pi} \cdot \dot{\boldsymbol{L}} \quad (4-28)$$

Where, $\bar{\boldsymbol{J}}_{pi} = \boldsymbol{J}_{pi} \cdot \bar{\boldsymbol{J}}$ represents the equivalent Jacobian inverse matrix between the velocity of the mass center of the piston rod and the linear velocity of the actuators.

4.2. Free-body analysis

4.2.1. Moving platform free-body analysis

Under the fixed coordinate system {A}:

The inertial force of the moving platform:

$$\boldsymbol{F}_B = -m_B \boldsymbol{a}_B \quad (4-29)$$

The inertia torque of the moving platform:

$$\boldsymbol{N}_B = -{}^A\boldsymbol{R}_B \cdot {}^B\boldsymbol{I}_B \cdot {}^{\boldsymbol{A}}\boldsymbol{R}_B^{\boldsymbol{T}} \boldsymbol{\varepsilon}_B - \boldsymbol{\omega}_B \times \left({}^A\boldsymbol{R}_B \cdot {}^B\boldsymbol{I}_B \cdot {}^{\boldsymbol{A}}\boldsymbol{R}_B^{\boldsymbol{T}} \cdot \boldsymbol{\omega}_B\right) \quad (4-30)$$

Where, ${}^B\boldsymbol{I}_B$ is the inertia matrix of the moving platform in the moving coordinate system {B}.

The gravity of the moving platform:

$$\boldsymbol{G}_B = m_B \boldsymbol{g} \quad (4-31)$$

The external force acting on the moving platform:

$$\boldsymbol{F}_W = {}^A\boldsymbol{R}_B {}^B\boldsymbol{F}_W \quad (4-32)$$

Under the fixed coordinate system {A}, The external torque acting on the moving platform:

$$\boldsymbol{N}_W = {}^A\boldsymbol{R}_B {}^B\boldsymbol{N}_W \quad (4-33)$$

4.2.2. Free-body analysis of cylinder and piston rod (actuator)

As shown in Fig. 6, a coordinate system is built on the cylinder and piston rod, Z_i axis of coordinate $\{C_i\}$ and $\widehat{\boldsymbol{s}}_i$ are in the same direction, Y_i axis of coordinate $\{C_i\}$ and $\boldsymbol{r}_{ai}$ are in opposite direction, X_i axis direction is determined by the Right-hand Rule. The coordinate transformation matrix of the coordinate system $\{C_i\}$ relative to the fixed coordinate system {A} is:

$${}^A\boldsymbol{R}_{Ci} = [\widehat{\boldsymbol{s}}_i \times \boldsymbol{r}_{ai}\widehat{\boldsymbol{s}}_i \times (\widehat{\boldsymbol{s}}_i \times \boldsymbol{r}_{ai})\widehat{\boldsymbol{s}}_i] \quad (4-34)$$

Under the fixed coordinate system {A}:

The inertial force of the cylinder is:

$$\boldsymbol{F}_{ci} = -m_{ci}\boldsymbol{a}_{ci} \quad (4-35)$$

The inertia torque of the cylinder is:

$$\boldsymbol{N}_{ci} = -{}^A\boldsymbol{R}_{Ci} \cdot {}^B\boldsymbol{I}_{ci} \cdot {}^{\boldsymbol{A}}\boldsymbol{R}_{Ci}^{\boldsymbol{T}} \boldsymbol{\varepsilon}_i - \boldsymbol{\omega}_i \times \left({}^A\boldsymbol{R}_{Ci} \cdot {}^B\boldsymbol{I}_{ci} \cdot {}^{\boldsymbol{A}}\boldsymbol{R}_{Ci}^{\boldsymbol{T}} \cdot \boldsymbol{\omega}_i\right) \quad (4-36)$$

The gravity of the cylinder is:

$$\boldsymbol{G}_{ci} = m_{ci}\boldsymbol{g} \quad (4-37)$$

The inertial force of the piston rod is:

$$\boldsymbol{F}_{pi} = -m_{pi}\boldsymbol{a}_{pi} \quad (4-38)$$

The inertial torque of the piston rod is:

$$\boldsymbol{N}_{pi} = -{}^A\boldsymbol{R}_{Ci} \cdot {}^B\boldsymbol{I}_{pi} \cdot {}^{\boldsymbol{A}}\boldsymbol{R}_{Ci}^{\boldsymbol{T}} \boldsymbol{\varepsilon}_i - \boldsymbol{\omega}_i \times \left({}^A\boldsymbol{R}_{Ci} \cdot {}^B\boldsymbol{I}_{pi} \cdot {}^{\boldsymbol{A}}\boldsymbol{R}_{Ci}^{\boldsymbol{T}} \cdot \boldsymbol{\omega}_i\right) \quad (4-39)$$

The gravity of the piston rod is:

$$\boldsymbol{G}_{pi} = m_{pi}\boldsymbol{g} \quad (4-40)$$

Based on the above free-body analysis, under the fixed coordinate system {A}, the equivalent driving force equation is established by the improved virtual work principle, and the driving force can be calculated.

Equivalent driving force converted from the external force on the moving platform:

Table 1
Coordinate of points on 3-RPS parallel robot.

Coordinate of points on 3-RPS parallel robot (unit/m)
${}^{A}a_1 = [0\ -2.11.336]^T$
${}^{A}a_2 = [-0.2082.135\ 0.03]^T$
${}^{A}a_3 = [0.208\ 2.135\ 0.03]^T$
${}^{B}b_1 = [0\ -2.11.25]^T$
${}^{B}b_2 = [-0.2082.057\ -0.056]^T$
${}^{B}b_3 = [0.208\ 2.057\ -0.056]^T$

Table 2
Structure parameters.

Parameters	Value
v_M/ (°/sec)	0.1
h_{ci}/ m	0.17
h_{pi}/ m	0.141
m_{ci}/ Kg	5.32
m_{pi}/ Kg	2.52
m_B/ Kg	1821.55
${}^{B}\boldsymbol{F}_W$	0
${}^{B}\boldsymbol{N}_W$	0
${}^{B}\boldsymbol{I}_B$/ (Kg·m^2)	$\begin{bmatrix} 3760 & 0 & 0 \\ 0 & 840 & 0 \\ 0 & -1070 & 3027 \end{bmatrix}$
${}^{B}\boldsymbol{I}_{ci}$/ (Kg·m^2)	$\begin{bmatrix} 0.048 & 0 & 0 \\ 0 & 0.048 & 0 \\ 0 & 0 & 0.0028 \end{bmatrix}$
${}^{B}\boldsymbol{I}_{pi}$/ (Kg·m^2)	$\begin{bmatrix} 0.02 & 0 & 0 \\ 0 & 0.02 & 0 \\ 0 & 0 & 0.0004 \end{bmatrix}$

Table 3
The trajectory of the moving platform.

Coordinates	Value
x/m	0
y/m	0
z/m	0.516
α/rad	0
β/rad	0.03 sin t
γ/rad	0.03 cos t

$$\boldsymbol{F}_{mB} = \bar{\boldsymbol{J}}^T \begin{bmatrix} \boldsymbol{F}_B + \boldsymbol{G}_B + \boldsymbol{F}_W \\ \boldsymbol{N}_B + \boldsymbol{N}_W \end{bmatrix} \quad (4\ -41)$$

Equivalent driving force converted from the external force on the cylinder and piston rod (actuator):

$$\boldsymbol{F}_{mi} = \bar{\boldsymbol{J}}_{ci}^T \begin{bmatrix} \boldsymbol{F}_{ci} + \boldsymbol{G}_{ci} \\ \boldsymbol{N}_{ci} \end{bmatrix} + \bar{\boldsymbol{J}}_{pi}^T \begin{bmatrix} \boldsymbol{F}_{pi} + \boldsymbol{G}_{pi} \\ \boldsymbol{N}_{pi} \end{bmatrix} \quad (4\ -42)$$

For the 3-RPS robot, the balance equation is established:

$$\boldsymbol{F} + \boldsymbol{F}_{mB} + \sum_{i=1}^{3} \boldsymbol{F}_{mi} = 0 \quad (4\ -43)$$

It can be explicitly expressed by:

$$\boldsymbol{F} = -\boldsymbol{F}_{mB} - \sum_{i=1}^{3} \boldsymbol{F}_{mi} \quad (4\ -44)$$

Where, $\boldsymbol{F}$ is the driving force of three actuators, $\boldsymbol{F} = [f_1 f_2 f_3]^T$.

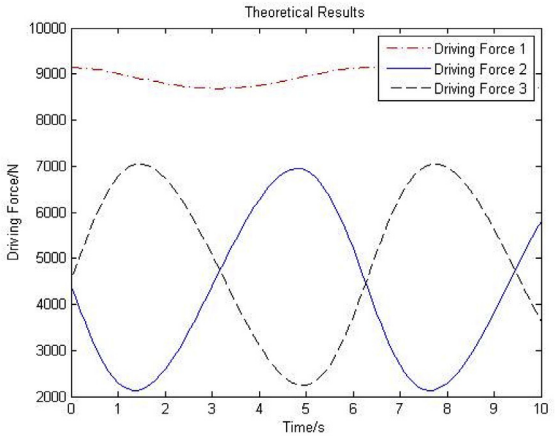

(a) Results of theoretical calculation in MATLAB

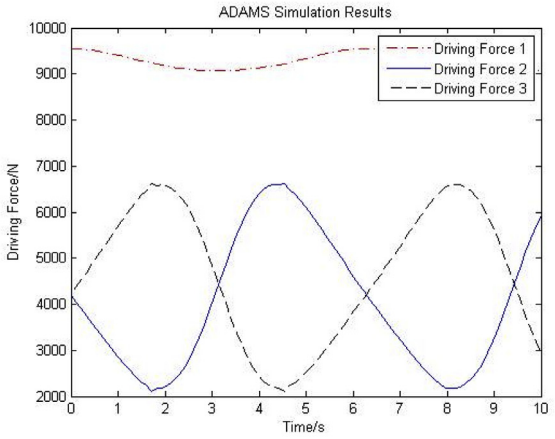

(b) Simulation result in ADAMS

Fig. 8. Comparison diagram of theoretical calculation and ADAMS simulation results. (a)Results of theoretical calculation in MATLA. (b)Simulation result in ADAMS.

5. Parameters of theoretical calculation and ADAMS simulation verification of 3-RPS parallel robot

After the model is established, the parameters are set as shown in Tables 1–1 and 1-2, and the trajectory of the moving platform is shown in Tables 1–3 (To highlight the change of driving force of hydraulic cylinder, the Euler angle motion function of moving platform is trigonometric function). In order to verifying the result in theoretical calculation, the model is simulated to obtain the driving force of the hydraulic cylinder.

According to the comparison of graph in MATLAB and ADAMS, the simulation data in ADAMS is essentially in agreement with the theoretical data (as shown in Fig. 8). However, the single most striking observation to emerge from the comparison is that there has a small mutation near the peak point in ADAMS simulation curve. After detailed analysis, it is found that the large mass of platform(1821.55 Kg) and the trigonometric function trajectory of moving platform are the main reasons cause the mutation of the curve. For the hydraulic cylinders, there are two completely different directions of motion near the peak point of the trigonometric function. The hydraulic cylinders are subjected to the large acceleration at this time. Moreover, such errors can also be eliminated by the parameter optimization in later work. The theoretical

basis for the stability control of the heavy-duty components driven by hydraulic cylinders is established.

6. Summarization and prospect

The structural design of divertor MFMP for CFETR was introduced in this paper. Aiming at the stable and reliable control requirements of the large heavy-duty divertor maintenance platform, the MFMP was simplified into 3-RPS parallel robot. By combining the Newton-Euler method and the improved virtual work principle, the equivalent Jacobian inverse matrix between each actuator and component was obtained to solve the driving force of each actuator. The theoretical basis for the stable control of the heavy-duty components driven by the hydraulic systems was obtained.

Aiming at the errors in ADAMS simulation, further studies, which take variables into account such as parameter optimization of model and parameter adjustment of simulation in ADAMS, will need to be undertaken.

Declaration of competing interest

The authors declare that they have no known competing financial interests or personal relationships that could have appeared to influence the work reported in this paper.

Acknowledgements

This work is supported by the National Natural Science Foundation of China No.11802305 and Engineering Design of CFETR Mainframe with Grant No. 2017YFE0300503. The authors would like to express their sincere gratitude to all the members of CFETR engineering design team.

References

[1] Jiangang Li, Yuntao Song, Yong Liu, et al., Main Engine Design of Experimental Reactor in Fusion Engineering, first ed., science press, Beijing, 2016.
[2] Y. Song, S. Wu, Y. Wan, et al., Concept design on RH maintenance of CFETR Tokamak reactor, Fusion Eng. Des. 9–10 (2014) 2331–2335.
[3] Wenlong Zhao, Yong Cheng, Xiaodong, et al., Reliability based assessment of remote maintenance system for CFETR divertor, Fusion Eng. Des. 146 (2019) 2777–2780.
[4] J. Li, Y. Wan, Present state of Chinese magnetic fusion development and future plans, J. Fusion Energy 38 (2019) 113–124.
[5] S. Yu, J. Lee, B. Park, et al., Ergonomic analysis of a telemanipulation technique for a pyroprocess demonstration facility, Nucl. Eng. Technol. 46 (2014) 489–500.
[6] Hocheol Shin, Seung Ho Jung, You Rack Choi, et al., Development of a shared remote control robot for aerial work in NPPs, Nucl. Eng. Technol. 50 (2018) 613–618.
[7] I.S. Kim, Y. Choi, K.M. Jeong, A new approach to quantify safety benefits of disaster robots, Nucl. Eng. Technol. 49 (2017) 1414–1422.
[8] Wenlong Zhao, et al., Concept design of the CFETR divertor remote handling system, Fusion Eng. Des. 98–99 (2015) 1706–1709.
[9] Rocco Mozzillo, et al., Concept design of DEMO divertor cassette remote handling: simply supported beam approach, Fusion Eng. Des. 116 (2015) 66–72.
[10] John J. Craig, Introduction to Robotics: Mechanics and Control, third ed., Prentice Hall, Upper Saddle River, 2005.
[11] C. Li, H. Wu, H. Eskelinen, et al., Design and analysis of robot for the maintenance of divertor in DEMO fusion reactor, Fusion Eng. Des. 146 (2019) 2092–2095.
[12] D. Hamid, Taghirad, Parallel Robots: Mechanics and Control, CRC, Boca Raton, 2013.
[13] Zhiyou Feng, Yonggang Li, Ce Zhang, et al., Research status and prospect of mechanism motion and dynamic analysis of parallel robot, China Mech. Eng. 9 (2006) 103–108.
[14] Bruno Siciliano, Oussama, Springer Handbook of Robotics, Springer, Heidelberg, 2008.
[15] N. Reza, Jazar, Theory of Applied Robotics, second ed., Springer, New York, 2010.
[16] Xiulong Chen, Tao Wang, Xiaoxia Liang, Qing Wang, Dynamic and static analysis of space 4-UPS/RPS parallel mechanism, J. Agric. Mach. 7 (2016) 398–406.
[17] F. Viganò, F. Escourbiac, S. Gicquel, et al., Structural analysis of the ITER Divertor toroidal rails, Fusion Eng. Des. 88 (2013) 2077–2083.
[18] N. Abhilash, Caro Stéphane, W. Philippe, Kinematic analysis of the 3-RPS-3-SPR series–parallel manipulator, Robotica, 2018, pp. 1–27.
[19] J. Gallardo-Alvarado, Posadas-García, Juan-de-Dios, Mobility analysis and kinematics of the semi-general 2(3-RPS) series-parallel manipulator, Robot. Comput. Integrated Manuf. 29 (2013) 463–472.
[20] D. Verdes, S.D. Stan, M. Manic, et al., Kinematics analysis, workspace, design and control of 3-RPS and TRIGLIDE medical parallel robots. 2nd International Conference on Human System Interaction, Catania, Italy, 2009. May 21-23.